Nanoscale

Accepted Manuscript

This article can be cited before page numbers have been issued, to do this please use: S. Bettini, S. Sawalha, L. Carbone, G. Giancane, M. Prato and L. Valli, *Nanoscale*, 2019, DOI: 10.1039/C9NR00951E.

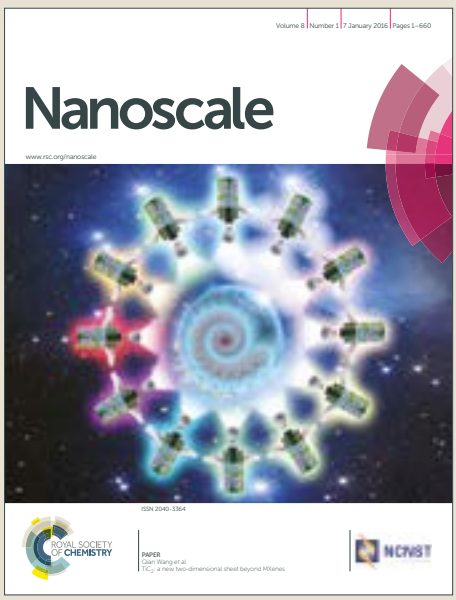




ROYAL SOCIETY OF CHEMISTRY

rsc.li/nanoscale

ROYAL SOCIETY OF CHEMISTRY
View Article Online
DOI: 10.1039/C9NR00951E

Journal Name

ARTICLE

# Carbon nanodots -based heterostructures for improving the charge separation and the photocurrent generation

Received 00th January 20xx,
Accepted 00th January 20xx

DOI: 10.1039/x0xx00000x

www.rsc.org/

Simona Bettini, [a, b] † Shadi Sawalha,[a, c] † Luigi Carbone,[d] Gabriele Giancane,[e, b*] Maurizio Prato,[f, g, h*] and Ludovico Valli [b, i]

The chance to employ carbon nanodots (CNDs) in solar devices was exploited combining them with a fulleropyrrolidine derivative (FP2). The interaction between the two species was promoted by the presence of opposite electrostatic charges on CNDs (negatively charged) and FP2 (positively charged). The supramolecular dyad CNDs/FP2 generation was induced at the air/water interface of a Langmuir trough: water soluble CNDs were dissolved in the subphase and FP2 chloroform solution was spread on the subphase; the electrostatic interaction promoted the formation of the supramolecular adduct FP2/CNDs, which was then transferred onto solid substrates. Photo-induced charge transfer was promoted in the FP2/CNDs dyad and we demonstrated that the presence of CNDs increased the short circuit current density under light illumination of a porphyrin – FP2/CNDs thin film of about 300% if compared with a more traditional porphyrin-FP2 solar device.

## Introduction

Several studies carried out on carbon-based nanomaterials such as graphene sheets[1,2], onion-like carbon[3,4], nanodiamonds[5,6], carbon nanotubes[7,8], fullerenes[9,10] and carbon nanodots (CNDs) [11,12] highlighted their multifaceted properties, proposing them as possible candidates for a wide variety of applications.[13] Among them, CNDs tuneable fluorescence emission[14] attracted the attention of many researchers since it allowed to propose such a material for bioimaging and biosensing applications. The tuneable fluorescence is a common characteristic of CNDs and of the most known semiconductor quantum dots such as CdSe, CdTe or PbS.[15] In contrast to inorganic quantum dots, CNDs are not dangerous for the human health and the use of heavy metals is not demanded for their production.[16–19]

Moreover, the chance to employ CNDs as a hole transporter material in solar cells was evaluated.[20] CNDs showed interesting properties as electron donors and electron acceptors, which make them suitable for photocatalysis applications and sensing device fabrication[21] as well as photoabsorption agents, sensitizers and transporting layer material in silicon-based hybrid solar cells,[22] and also, in combination with $TiO_2$,[23,24] in presence of inorganic quantum dots[25], dyes[26] and organic polymers[27] in solar devices.[28,29]

In the present work, the formation of a supramolecular adduct between a double positively charged fulleropyrrolidine derivative (FP2) and negatively charged CNDs was promoted both in solution and at the air-water interface in a Langmuir trough[30]. The supramolecular adduct was transferred by means of the Langmuir-Schaefer method[30] employing the electrostatic interaction between the amphiphilic FP2 and the water soluble CNDs. The dyad fulleropyrrolidine derivative/carbon nanodots was characterized in solution by means of UV-Vis, FTIR and fluorescence spectroscopies. Also, the dyad's floating films were studied by means of surface pressure *vs* area per molecule Langmuir isotherm, reflection spectroscopy and Brewster Angle Microscopy. Afterwards, films of dyad samples were transferred onto diverse solid substrates for transmission electron microscopy (TEM), UV-Vis absorption and fluorescence emission investigations. Finally, the photo-induced charge transfer phenomenon in the Langmuir-Schaefer FP2/CNDs dyad was studied by means of a home-made ITO/(active layer)/$I^-$, $I_3^-$/Pt-ITO cell. The presence of CNDs allowed increasing the charge transfer efficiency of about 300% when short circuit current density under light

[a] Department of Innovation Engineering, Università del Salento, Via Monteroni, I-73100 Lecce, Italy.
[b] Consorzio Interuniversitario Nazionale per la Scienza e Tecnologia dei Materiali, INSTM, Via G. Giusti, 9, I-50121 Firenze, Italy.
[c] Chemical Engineering Department, An-Najah National University, Nablus, Palestine
[d] . CNR NANOTEC-Institute of Nanotechnology, C/o Campus Ecotekne, University of Salento, Via Monteroni, Lecce, 73100, Italy
[e] Department of Cultural Heritage, Università del Salento, Via D. Birago, 48, I-73100 Lecce, Italy, gabriele.giancane@unisalento.it
[f] Center of Excellence for Nanostructured Materials (CENMAT), INSTM UdR di Trieste, Dipartimento di Scienze Chimiche e Farmaceutiche, University of Trieste, Piazzale Europa 1, Italy, prato@units.it
[g] Carbon Nanobiotechnology Laboratory, CIC biomaGUNE, Paseo de Miramón 182, San Sebastian, Spain
[h] Basque Fdn Sci, Ikerbasque, 48013 Bilbao, Spain
[i] Department of Biological and Environmental Sciences and Technologies, Università del Salento, Via Monteroni, I-73100 Lecce, Italy
† These authors equally contributed.
Electronic Supplementary Information (ESI) available: [details of any supplementary information available should be included here]. See DOI: 10.1039/x0xx00000x

DOI: 10.1039/C9NR00951F

illumination of a porphyrin – FP2/CNDs thin film is compared with a more traditional porphyrin-FP2 solar device.

## Methods

All reagents and solvents were purchased from commercial sources and used without purification. MilliQ grade (18.2 mΩ·cm resistivity) water was used in all the Langmuir experiments. The commercial porphyrin derivative 5,10,15,20-Tetra(4-pyridyl)-21H,23H-porphine (TPyP hereafter) was purchased from Sigma Aldrich and used without further purification (chemical structure is reported in Figure S1). Double positively charged amphiphilic fulleropyrrolidine (FP2 hereafter) was synthetized in accordance with the procedure reported in Mateo-Alonso and co-workers [31] and its chemical structure is reported in the Figure S2.

### Synthesis of Carbon nanodots

CNDs were prepared according to the method reported by Dong and co-workers[32]: 3 mL of ethanolamine were mixed with 4.5 mL of 30% hydrogen peroxide and the solution heated at 250°C in air for 7 min. Because of the oxidant action, the colour of ethanolamine solution changed from colourless to bright yellow after the addition of $H_2O_2$. The reaction product was cooled at room temperature and dispersed in 200 mL distilled water. The CNDs solution was filtered through 0.45 µm PETE hydrophilic filter, centrifuged at 8000 rpm (9900 rcf) by means of a Hettich Mikro 120 Benchtop Centrifuge for one hour and the supernatant recovered thereafter. The solution was stored in dark at 4°C for further uses.

### Carbon nanodots characterizations

CNDs, TPyP and FP2 were characterized by means of FTIR, UV-Visible and fluorescence spectroscopies. Infrared characterizations were performed by a Perkin Elmer Spectrum One in ATR (Attenuated Total Reflection) mode and 64 scans were acquired in the range 4000 $cm^{-1}$-800 $cm^{-1}$ for each sample.

Varian Cary 5000 was used to record the UV-Visible spectra of the species both in solution and transferred as thin film on solid quartz substrates.

Steady-state fluorescence spectra were registered by a Horiba FluoroLog.

ζ-Potential measurements of samples dissolved in ultrapure water were performed by using Zetasizer Nano-ZS90 (Malvern Instruments Ltd, Malvern, UK).

X-ray photoelectron spectroscopy (XPS) was performed by means of a X-ray Photoelectron Spectroscopy (Electron Spectroscopy for Chemical Analysis, ESCA) A SPECS SAGE HR 100 system equipped with a 100 mm mean radius PHOIBOS analyzer with MgKα X ray source. To carry out the XPS investigation, CNDs were deposited on titanium coated glass substrate. Finally, the XPS spectra were analyzed and deconvoluted by means of CasaXPS software.

Low-magnification TEM analysis of CNDs and FP2/CNDs dyads was performed using JEOL JEM-1011 (JEOL, Tokyo, Japan) operating at 100kV and equipped with a CCD camera (Gatan Orius 831). FP2/CNDs dyad samples for investigation were deposited via a LS procedure, employing carbon-coated Cu grids as collecting substrates. Subsequently, the specimens were dried at 60°C overnight before analysis.

### Langmuir through experiments

Supramolecular dyad of FP2/CNDs was assembled at the air/aqueous subphase interface. A NIMA trough apparatus (area of 415 $cm^2$) was used in the Langmuir experiment. Amphiphilic and pseudo amphiphilic species, FP2 and TPyP respectively, were spread from chloroform solution onto the surface of the subphase by means of a gas-tight syringe. After the solvent evaporation, in a typical Langmuir experiment[33], two Teflon-made barriers that graze the subphase surface, were moved at a speed of 7 $cm^2$ $min^{-1}$, in order to reduce the area occupied by the floating film. During the barriers' motion the surface pressure of the floating film was recorded by means of a paper-made Wilhelmy plate and the so called surface pressure *vs* area per molecule Langmuir isotherm was obtained.[34]

The NIMA Langmuir trough is equipped with a Brewster Angle Microscope (BAM), which allows monitoring the floating film morphology during its formation, promoted by the barriers' movement. Furthermore, the same Langmuir trough is equipped with two optical fibers to perform reflection spectroscopy.[35] According to previously reported results[36], TPyP was dissolved in chloroform at a molar concentration of $1.6 \times 10^{-4}$ M and transferred at 18 mN/m through a Langmuir-Schaefer method, whilst FP2 was dissolved in chloroform at a final concentration of $1.2x10^{-4}$ M and transferred, according to [37], at 18 mN/m.

Quartz and ITO substrates were hydrophobized, before carrying out the deposition, by overnight exposure to 1,1,1,6,6,6-hexamethyldisilazane vapours in a desiccator.

As above detailed, all the Langmuir films were transferred by means of the Langmuir-Schaefer (LS) technique, the horizontal variation of the Langmuir-Blodgett (LB) method, since the one did not allow to obtain uniform films and very low transfer ratios were recorded.[30]

### Photoelectrochemical Measurements

The photoactivity of the LS layers was monitored by means of a home-made ITO/(active layer)$_n$/$I^-$,$I_3^-$/Pt-ITO cell.[38]. The ITO substrate (purchased from Sigma Aldrich, 8-12 Ω/sq), herein used as a counter electrode, was drilled to create a 1 mm diameter hole to allow the injection of the electrolyte. Then, the Pt catalyst was deposited on the ITO glass, by casting a drop of $H_2PtCl_6$ solution (2 mg Pt in 1 mL of ethanol), and heated at 400°C for 15 min. The ITO/(active layer)$_n$ electrode and Pt-counter electrode were assembled into a sandwich-type cell and sealed with a hot-melt gasket of 25 mm thickness made by the ionomer Surlyn 1702 (Dupont). The used photoactive film area used was 0.3 $cm^2$ and an electrolyte drop was put from the back side of the ITO counter electrode. An acetonitrile solution containing LiI (0.5 M) and $I_2$ (0.01 M) was employed as electrolyte. Finally, the hole in the counter electrode was sealed using the hot-melt Surlyn and a cover glass. A Keithley 2400 multimeter and a PGSTAT100 Autolab

potentiostat were utilized for recording the JV curves. A 1.5 AM LOT-Oriel Solar S class A solar simulator was used for the illumination. The IPCE was calculated with the following equation: IPCE (%) = 124 000 · I/(λ · f(λ)) where λ is the light wavelength (measured in nm) selected by means of an Omni-λ 1509 monochromator with a step of 20 nm, I is the photocurrent density (A $cm^{-2}$) and f(λ) is the incident-light power density at wavelength λ (W $cm^{-2}$) calibrated using a radiant-power/energy meter before each experiment.

## Results and discussions

### Characterization of the synthetized carbon nanodots

The CNDs formation was monitored by means of ATR-FTIR and UV-visible spectroscopy (Figure 1, box a and b, respectively). Figure 1a reports the FTIR spectra obtained for ethanolamine (black line), synthesis intermediate-products (red line) and CNDs (blue line), respectively. The ethanolamine spectrum is dominated by the C-O stretching modes and in particular by the C-O-H signal located at about 1031 $cm^{-1}$. [39] Upon reaction advancement, this component progressively reduces till completely disappears in the CNDs spectrum (blue line). Further confirmation could be obtained observing the strong reduction of O-H stretching modes region at high wavenumbers (3600-3150 $cm^{-1}$)[39]. A similar rationale can be proposed about primary amine group vibrations, whose signals almost disappeared. Indeed, the CNDs spectrum lacks the $NH_2$ bending modes located in the region between 900 and 700 $cm^{-1}$, the correspondent stretching modes, the asymmetric and the symmetric ones at 3760 and 3290 $cm^{-1}$, respectively, the 3200 $cm^{-1}$ signal due to the Fermi resonance, and the intense overtone located at about 1600 $cm^{-1}$.[39] The almost complete lack of OH and $NH_2$ signals, together with the strong reduction of the CH bending modes (1470-1200 $cm^{-1}$)[39] clearly confirmed the successful occurrence of the oxidation process. In fact, the intermediate spectrum (red line) clearly shows the presence of the typical vibration modes of an oxidized amidic group, and in particular the bands due to C=O stretching (1660 $cm^{-1}$), to N-H bending (1570 $cm^{-1}$) and at about 1380 $cm^{-1}$ to N-O symmetric stretching modes are evident. [32] The presence of the amidic group is in perfect agreement with the reaction advancement, which involves a first step of polymerization among ethanolamine and its oxidative products, upon $H_2O_2$ action, inducing the formation of amidic bonds as crosslinkers[32]. Then, the carbonization takes place and those signals almost completely disappear and the FT-IR spectrum of CNDs (blue line) results dominated by C=O stretching mode (1660 $cm^{-1}$)[39] and the C-O stretching mode of the aryl ether (=C-O-C-, 1067 $cm^{-1}$) bands[40]. The development of ether polar functional groups promotes the solubility of CNDs in water.[40] The CNDs surface electrostatic charge was measured by means of ζ-potential method and a -22 mV negative charge was recorded in MilliQ grade water.

UV-Vis spectroscopy characterization confirmed the results obtained by FT-IR characterization. The presence of C=O and N=O functional groups during the polymerization phase was attested by the presence of the absorption peak located at 280 nm, which is normally referred to the n-π* transition of C=O or N=O[41,42], in the spectrum of the intermediate product (red line, Figure 1b). This peak intensity decreased during the carbonization step with the formation of the CNDs (blue line, Figure 1b). A broad weak absorption peak is centred at nearly 370 nm referred to energy trapping states located on the particle surface, which can lead to the noticed fluorescence of carbon dots (Figure 1b).[13] XPS analysis was carried out to investigate the surface groups of the prepared CNDs. Figure S3a reports the obtained XPS survey spectrum, showing that CNDs are composed of carbon, oxygen and nitrogen with an atomic percent of 60.21, 23.69 and 16.11, respectively. The high resolution C1s spectrum Figure S3b could be deconvoluted into 3 peaks at 285, 286 and 287.8 eV, which are referred to C-C, C-O/C-N and C=O/C=N groups respectively.[43,44] The O1s spectrum (Figure S3c) reveals the presence of C=O at 531 eV and of C-OH/C-O-C at 532.2 eV.[45] The presence and the dissociation of these oxygenated functional moieties lead to a negative surface charge of the CNDs,[46] according to ξ-potential analysis (-22 eV). Finally, N1s spectrum (Figure S3d was deconvoluted into a main peak at 399.3 eV, which can be ascribed to pyridinic nitrogen groups; the other peak shown at 401.9 eV represents the N-H group.[32]

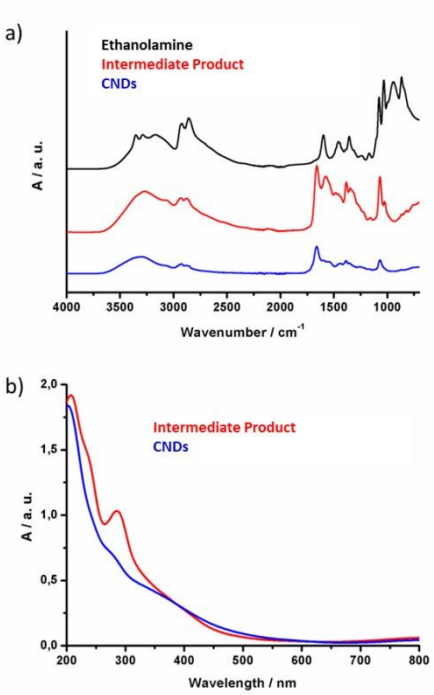


**Figure 1. a) FTIR spectra of ethanolamine, intermediate products and CNDs; b) UV-Vis absorption spectra of intermediate product and CNDs.**

Fluorescent emission properties analysis represents a key characterization technique for CNDs[47]. In fact, changes of the emission frequency as a function of the excitation wavelength are a rather common finding for CNDs.[48,49] A typical experiment was carried out by analysing the emission spectra of a 0.05mg/mL CNDs aqueous solution changing the

View Article Online
DOI: 10.1039/C9NR00951E



excitation wavelength from 320 nm to 460 nm with a step of 20 nm. As illustrated in Figure 2a, a maximum emission at about 460 nm was recorded upon 380 nm excitation. By exciting from 320 to 380 nm,[49] the CNDs emission intensity increased. The maximum emission wavelength shifted to lower energy values with a simultaneous decrease of the fluorescence intensity as excitation wavelengths higher than 380 nm were used.[49]. Such an effect is usually attributed to the influence of the energetic defects on the CNDs surface on energetic levels,[32,42,50] as well as the size and the size distribution can influence the recombination processes, even among different CNDs, strongly affecting the emission features.[51]

The synthesized CNDs exhibited good up-conversion fluorescent properties with an emission peak at about 470 nm (Figure S4) as typically observed for the CNDs. [50,51,53]

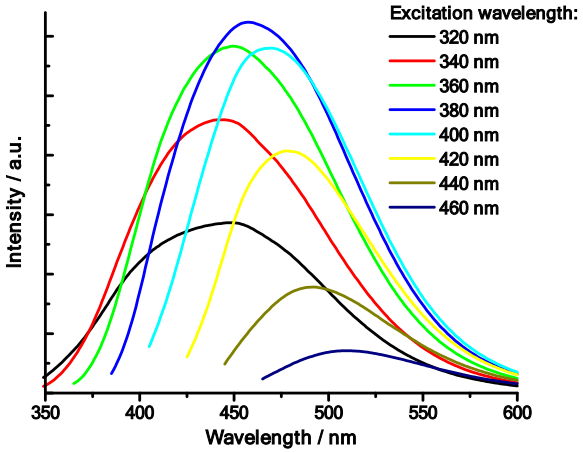


**Figure 2. a) Fluorescence emission of CNDs obtained at different excitation wavelengths**

TEM images of the cast film of CNDs were recorded and the typical morphology of CNDs was pointed out (Figure 3).[54,55] Size distribution (inset in Figure 3) highlighted small nanostructures with an average diameter of about 3 nm.

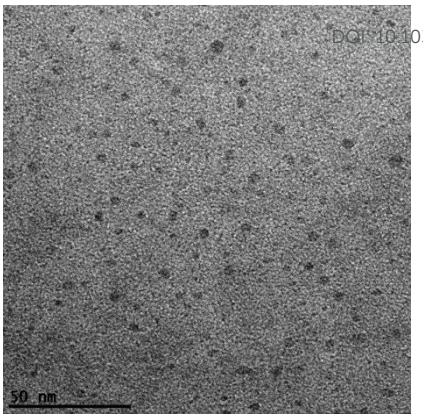


**Figure 3. TEM image of the as-prepared CNDs. The size-distribution of the CNDs is reported in Figure S5.**

**FP2/CNDs supramolecular dyad characterization**

The interaction among the doubly-charged fulleropyrrolidine derivative and the CNDs was evaluated by monitoring the fluorescence emission variations of CNDs in presence of FP2. In a typical titration experiment, different volumes of a $1.4 \times 10^{-3}$M FP2 solution in ethanol/water 50/50 (vol/vol), were added to CNDs aqueous solution at a fixed concentration of 0.05 mg/mL. Fluorescence emission was recorded at an excitation wavelength of 380 nm and an evident quenching of the fluorescence intensity has been obtained as the FP2 concentration increases (Figure 4a). The absorption of FP2 at 380 nm can be neglected and the total photon incident on CNDs can be considered a constant (Figure S6). The rationale is an energetic and/or electronic intercommunication that takes place between the two species.[56] As a further confirmation of this rationale, the upconversion emission of CNDs was monitored increasing the FP2 concentration (Figure S7). The communication between the two species and the upconversion of the energy of the absorbed photon act as competitive mechanisms: the charge transfer from CNDs towards FP2 reduces the electron available to relax at the fundamental level and, of course, the upconversion efficiency. Furthermore, experimental data graphed in the Stern-Volmer plot (Figure 4b) could not be fitted by a linear relation, suggesting that a combined effect of dynamic and static quenching could rule the CNDs fluorescence decrease[57]. According to the results reported by Das and co-workers about the graphene quantum dots fluorescence quenching promoted by single walled carbon nanotubes [58], CNDs fluorescence quenching was fitted with a compressed-exponential growth, as follows:

$$\frac{I_0}{I} = \exp\left(b[Q]\right)^a$$

where $I_0$ represents the maximum fluorescence emission without quencher, $I$ the fluorescence intensity in presence of FP2, $b$ and $a$ are two constants.

The fitting of the experimental data provided $a$=1.643 and $b$=0.018, two values indicative of an unusually high fluorescence quenching, if compared with the modified Stern-Volmer equation where $a$ is equal to 1 [57]. This outcome can be

explained as a consequence of the strong interaction between FP2 and CNDs in the formation of the supramolecular adduct.[58]

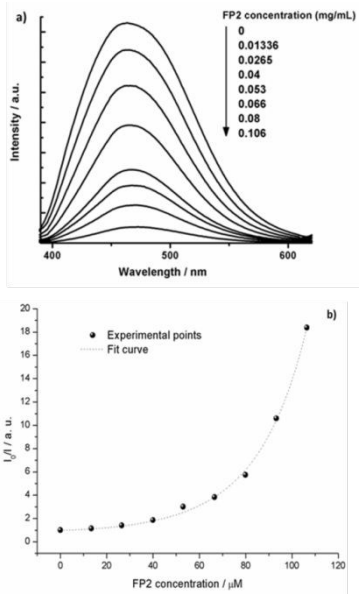


**Figure 4. a) CNDs fluorescence quenching vs increased amount of FP2. b) Stern-Volmer plot of the fluorescence intensity decrease of carbon nanodots as a function of FP2 concentration. The experimental points were fitted by means of a compressed-exponential growth curve (R square=0.998).**

### FP2/CNDs dyad floating film formation

The possibility to promote the carbon nanodots/fulleropyrrolidine derivative supramolecular adduct formation was evaluated using a Langmuir trough. Several examples of supramolecular adducts have been promoted and studied at the air/water interface [59,60] . Chelation [61,62], electrostatic interaction [63,64] and other supramolecular interactions [65] between a water dissolved species and a floating amphiphilic (or pseudo-amphiphilic) molecule can be used as driving force to induce the formation of host-guest adducts. Langmuir method, even though not particularly suitable for the deposition of large area solid films, appears particularly interesting for promoting self-aggregating supramolecular structures. In fact, the possibility to use the minimization of free energy of the molecules at the air-subphase interface allows to obtain very appealing supramolecular adducts that show unique characteristics [67–69] and, as reported in the present case, it is possible to promote the formation of supramolecular dyads and triads with substances soluble in different solvents. Furthermore, the accurate control of the deposition parameters allows to transfer solid films with a very high reproducibility.

CNDs were dissolved, in different concentrations, in ultrapure water and the carbon nanodots solutions were used as the subphases in the Langmuir experiments. Three different concentrations of CNDs in water subphase were selected in order to check the effect of carbon nanodots concentration on the supramolecular adduct FP2/CNDs formation. In particular, concentration values of 0.05 mg/mL, 0.15 mg/mL and 0.44 mg/ml were used as subphase with a practical focus towards the first one, which was selected as it corresponded to the amount used in the PL quenching experiments. We observed that CNDs concentrations higher than 0.2 mg/mL significantly and negatively affected the uniformity of the deposited FP2/CNDs films. Hence, air/subphase experiments were carried out by evaluating 0.05 mg/mL and 0.15 mg/mL CNDs concentrations solely.

An amount of 120 μL of FP2 chloroform solution ($1.2\times10^{-4}$ M) was spread, by means of a glass syringe, onto the aqueous subphases and the surface pressure *vs* area per molecule Langmuir isotherms were recorded. FP2 molecules spread onto the ultrapure water subphase (blue line in Figure 5), as already discussed in a previous work[37], suggesting the formation of a stable Langmuir monolayer at the air/water interface. The presence of the two positive electrostatic charges on the fulleropyrrolidine molecules inhibits the attitude of $C_{60}$ derivative to aggregate. Nevertheless, BAM images of FP2 films floating onto ultrapure water showed, even at low surface pressure values, the formation of bright spots as a clear consequence of small FP2 aggregates (Figure 6a). The presence of the CNDs in the subphase, at both 0.05 and 0.15 mg/mL concentrations, brings about a shift toward larger areas per molecule. In particular, from 90 Å² to 120 Å² for the subphase containing 0.05 mg/mL CNDs (black line in Figure 5) and up to 160 Å² for the 0.15 mg/mL carbon nanodots subphase (red line in Figure 5). Also, a slope change of the Langmuir isotherm is recorded at 28 mN/m when 0.05 mg/mL CNDs subphase is used and at about 38 mN/m in the case of 0.15 mg/ml CNDs subphase. The smoother phase transition observed in the case of the FP2 Langmuir film spread on the aqueous subphase containing 0.15 mg/mL CNDs is a consequence of a less rigid FP2 floating film: CNDs work as a spacer between FP2 molecules, allowing the re-arrangement of the C60 derivative floating molecules under the barriers' effect. These observations further confirm the interaction among the water dissolved species and the floating molecules.

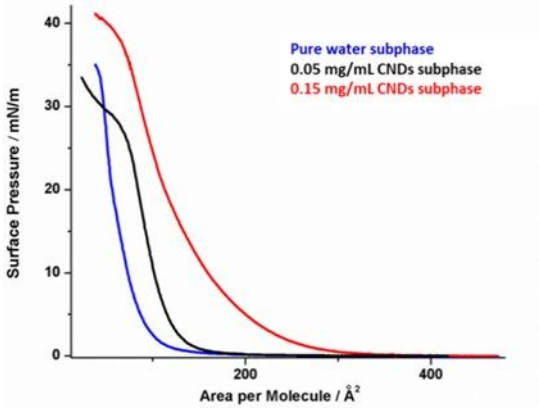


**Figure 5. Surface pressure vs area per molecule Langmuir isotherms of FP2 spread onto air-subphase interface of pure water subphase (blue line), 0.05 (black curve) and 0.15 mg/mL (red line) CNDs subphases.**

View Article Online
DOI: 10.1039/C9NR00951E



Brewster Angle Microscopy confirmed that the presence of CNDs dissolved in the subphase influences the FP2 floating film formation (Figure 6b and 6c). In fact, the simultaneous presence of not covered areas of the subphase and Langmuir film regions were formed even at low surface pressure values when the FP2 was spread on the ultrapure water subphase; on the contrary, when carbon nanodots are in the subphase, an almost complete coating of the interface was reached at 4.5 mN/m. The rationale is that under the barriers' motion, the presence of CNDs ensures the formation of thicker floating films as highlighted by the grey light grade of the floating film recorded by BAM.

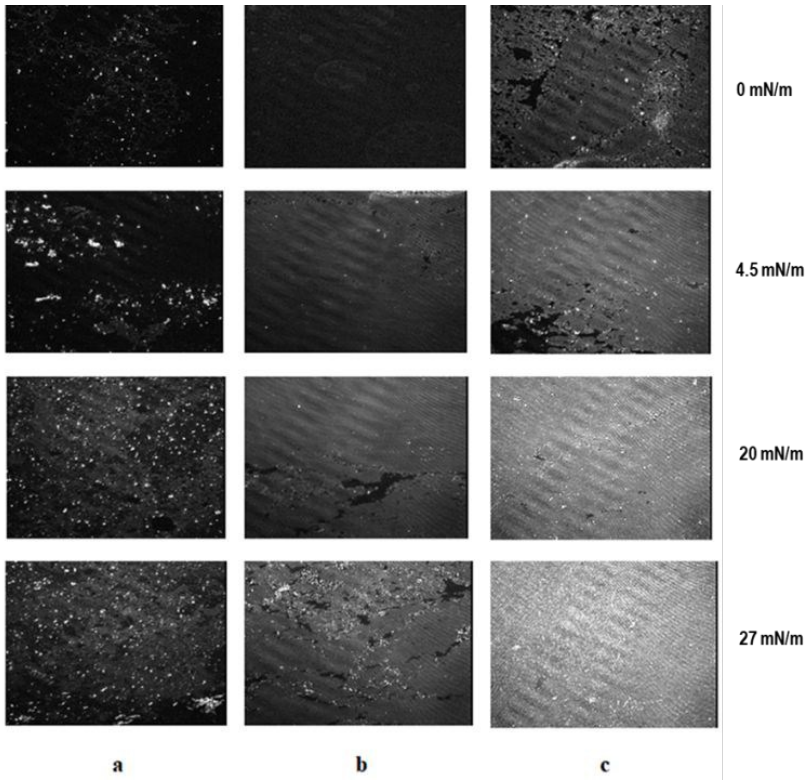


**Figure 6. BAM pictures of FP2 Langmuir film formed on ultrapure water (column a), on 0.05 mg/mL CNDs subphase (column b) and on aqueous subphase containing 0.15 mg/mL solution of carbon nanodots (column c) acquired at different surface pressures.**

Floating films were further characterized by means of the reflection spectroscopy at the air/subphase interface (Figure S8). Reflection variation $\Delta R$, for thin films, is directly proportional to the absorbance of the floating film, therefore, the reflection spectrum provides the same information that can be obtained from an absorption spectrum [63]. Typical fulleropyrrolidine thin film reflection spectra were recorded, even though it is relevant to observe that a well-defined reflection band appeared at 425 nm; the nature of this peculiar band will be discussed in the next paragraph.

**FP2/CNDs adduct transfer on solid substrates**

The LS method was used to transfer the FP2/CNDs adduct generated at the air/subphase interface. The LS method was used since the FP2 floating film appeared too rigid to be transferred by means of the usual LB approach[30]; indeed, very low deposition rates and not uniform solid films were obtained when the traditional vertical deposition method was adopted. LS method allows the formation of self-promoted supramolecular adduct and the simultaneous transfer of two species with very different solubility. The opposite electrostatic charges present on the two species is the driving force that promotes the formation of supramolecular adduct, giving to the molecules the chance to minimize their free-energy during the formation of the dyad. The UV-visible spectrum of the film obtained by transferring FP2 from the water subphase and containing CNDs with a concentration of 0.15 mg/mL, evidence the peculiar presence of an absorption band centred at 427 nm (Figure 7a). The intensity of this absorption band is proportional to the number of performed LS runs (Figure 7b) and, interestingly, this band has not been observed in the visible spectrum of the FP2 LS films (Figure 7c) or in the spin coated film of the mixture FP2/CNDs (Figure 7c).

View Article Online
DOI: 10.1039/C9NR00951E



Furthermore, it is worth to observe that this new band is barely visible when FP2 Langmuir films are transferred from water subphase, containing CNDs at a concentration of 0.05 mg/mL (Figure 7d).

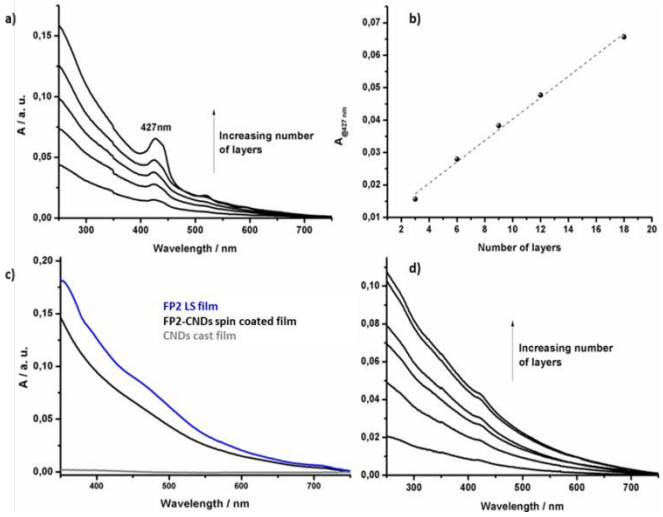


**Figure 7. a) Visible spectra of the FP2/CNDs thin films of increasing number of layers (dyad was transferred from a water subphase containing 0.15 mg/mL CNDs). b) The proportional relation between the absorption intensity recorded at 427 nm and the number of LS layers confirms the good repeatability of the deposition process. c) Absorption spectra of LS film of FP2 (blue line), spin coated film of FP2/CNDs (black line) and CNDs cast film (grey line). d) Visible spectra of Langmuir films transferred from water subphase containing CNDs at a concentration of 0.05 mg/mL.**

All such evidences prove that both the concentration of the carbon nanodots in the subphase and the film transfer method are crucial for originating and transferring the supramolecular adduct FP2/CNDs. A possible rationale of this new absorption band could be proposed by considering the opposite electrostatic charges of FP2 and CNDs. The interaction between the floating molecules and the CNDs dissolved in the water subphase probably induce a partial neutralization of the positive charges on the fullerene derivatives. This allows the formation of FP2 aggregates promoted by the significant Van der Waals forces that rule the aggregation phenomena in $C_{60}$ and its derivatives [69]. In this view, the appearance of absorption bands between 400 and 500 nm in the visible spectra of $C_{60}$ derivatives, is usually attributed to aggregation forms of fullerene [72], in particular when these are transferred onto solid films [73]. The absence of the absorption band at 427 nm in the spectra of the FP2/CNDs spun-coated film could be attributed to a phase separation occurring between FP2 and CNDs because of the low mutual miscibility of both solutions. Consequently, the electrostatic repulsion generated by the positive charges on the fulleropyrrolidine functionalization, reduce the $\pi$-$\pi$ interactions among the FP2 molecules.

Just one LS run of the dyad FP2/CNDs was carried out by transferring FP2 from the water subphase containing CNDs with a concentration of 0.15 mg/mL directly onto Cu TEM grids to morphologically characterize the deposited adducts (Figure 8 and Figure S9).

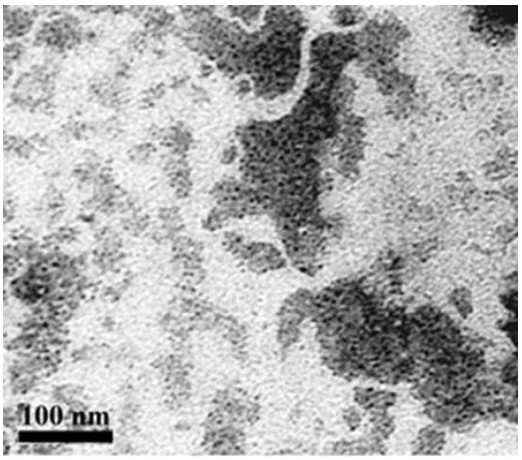


**Figure 8. TEM picture of 1 LS run of FP2/CNDs dyad obtained by transferring FP2 from a water subphase containing 0.15 mg/mL of CNDs.**

The picture shows that the substrate is not homogenously covered and segregated and distributed domains of organic material, presumably FP2, are well visible. It is worth underlining as CNDs, which appear as black spots, are not spread on the surface, but embedded into those islands of organic materials, confirming the success of the deposition procedure, which ensures the formation of a stable supramolecular adduct and the subsequent transfer onto a solid supports.

**Photoinduced phenomena in the FP2/CNDs supramolecular adduct**

FP2/CNDs dyad was transferred directly onto ITO substrates and a home-made electrochemical cell was assembled as reported in the experimental section. JV characteristics acquired using the supramolecular adduct as active layer showed the typical diode profile and a photoactivity can be observed when the device was illuminated with AM 1.5 solar simulator (Figure S10). Although very low, a short circuit current density ($J_{SC}$) of about 13.5 $\mu A\ cm^{-2}$ has been measured. It can be supposed that a charge transfer phenomenon from CNDs towards fullerene derivatives occurs [58,72]. This rationale is also corroborated by the already observed fluorescence quenching.

A low photoactivity of FP2 LS film (Figure 9a) has been noticed as a consequence of the electron transfer after the photon excitation between fullerenes [73] and fullerene aggregates [76]. The well-known behaviour of the carbon nanodots films as hole transporter material enhances the electron-hole separation and the charge transport and, consequently, the short circuit current (Figure 9a) [75].

The efficiency of photocurrent generation was further improved by adding, to the FP2/CNDs layer, a light harvesting molecule. Porphyrin derivatives are a class of compounds widely used as a photon harvesting material able to transfer one (or more) electrons to suitable materials [76-78]. TPyP (see Materials section) was used as a light antenna and electron donor species. It is well-known that porphyrins can transfer, under illumination, electrons towards fullerene derivatives and other allotropic forms of the carbon. Therefore, it has been argued that the presence of TPyP should increase the photocurrent values when one layer of porphyrin was transferred on each layer of FP2/CNDs (inset Figure 9b). The porphyrin derivative was in the past characterized at the air/water interface [31] and transferred at a surface pressure value of 18 mN/m. According to the results reported in 31, surface pressure value of 18 mN/m is compatible with a model of the spread molecules where the porphyrin rings lye on the subphase surface in a playing card arrangment.[36] Porphyrin derivative Langmuir film was then transferred onto ITO solid support by means of the LS method and then the FP2/CDNs adduct obtained at the air/subphase interface of another Langmuir trough was transferred on the TPP LS layer. This configuration was adopted in order to maximize the interface between the electron donor specie (TPP) and the electron acceptor supromolecular adduct (FP2/CNDs). The Langmuir-Schaefer technique allowed to transfer the TPyP layer without affecting the supramolecular dyad's layer while ensuring the control of the deposition parameters of TPyP LS film. The procedure was repeated 8 times and eight alternate layers TPyP-FP2/CNDs were transferred and the absorption (in Figure S11 the absorption spectra of FP2-CNDs and TPyP/FP2-CNDs 8 LS layers are reported) and fluorescence emission ($\lambda_{exc}$=440 nm) ~~was~~ were monitored. As reported in Figure S12, even though TPyP is transferred on FP2/CNDs layer, the reproducibility of the deposition process is not affect and the linear correlation between the TPyP maximum absorption and the number of LS layers confirms the reproducibility and the accurate control of deposition procedure. The presence of the supramolecular FP2/CNDs dyad partially quenches the porphyrin derivative fluorescence (Figure 9b) and light-assisted enhancements of the short circuit current of about 160% (compared with FP2/CNDs) and 290% (compared with TPyP-FP2) have been obtained (Figure 9a) as a consequence of the increased light harvesting induced by the presence of the porphyrin derivative layer. It is worth observing that the TPyP fluorescence quenching is similar in the case of FP2 (black spectrum) and in presence of the supramolecular dyad FP2/CNDs (red line). This evidence suggests that the light induced charge transfer from porphyrin takes place exclusively towards FP2. Nevertheless, it is relevant to observe that the $J_{SC}$ value recorded for the TPyP-FP2/CNDs, that is 21.8 $\mu A/cm^2$, is equal to the sum of the short circuit currents of FP2/CNDs and TPyP/FP2 (7.5 $\mu A/cm^2$) suggesting that probably two different charge transfers take place in the triad TPyP-FP2/CNDs: one from the porphyrin to the fullerene and the other one from the CNDs to the fullerene.

Photoaction spectra of only 8 alternate layers of TPyP/FP2 dyad and 8 alternate layers TPyP/FP2-CNDs triad were recorded in presence of a monochromatic light (see Photoelectrochemical Measurements paragraph). Incident photon to current efficiency (IPCE) shows a maximum for both the systems centred at the Soret band of porphyrin derivative, suggesting that the predominantly active component is the TPyP. Furthermore, an increasing of IPCE value is observed at low wavelength confirming a charge transfer from CNDs toward the fulleropyrrolidine derivatives. The maximum IPCE for both the system is about 0.35%.

The device stability to different on-off cycles was verified illuminating the TPyP-FP2/CNDs for 5 sec and recording the current density (figure S13) and no relevant variation in the short circuit current density was observed during 50 cycle.

Finally, TPyP-FP2/CNDs LS films were dark stored at room temperature and their photo-responses checked over 16 days. After each experiment the substrates were three times washed with ultrapure water in order to remove the electrolyte and then dried under nitrogen flux. A worsening of the current density was observed after the fifth day, reasonably because a partial desorption of the active layers during the substrate washing steps.

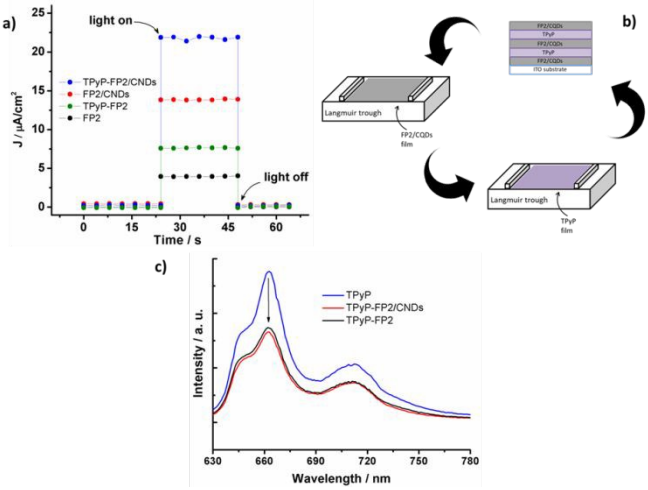


**Figure 9. a) Photocurrent generation from the LS films of TpyP-FP2/CNDs, FP2/CNDs and FP2. b) Fabrication of the photodevices carried out by the deposition of the triad TPyP-FP2/CNDs. c) Fluorescence quenching of TPyP in presence of FP2 (black spectrum) and FP2/CNDs (red spectrum) when transferred on quartz substrate.**

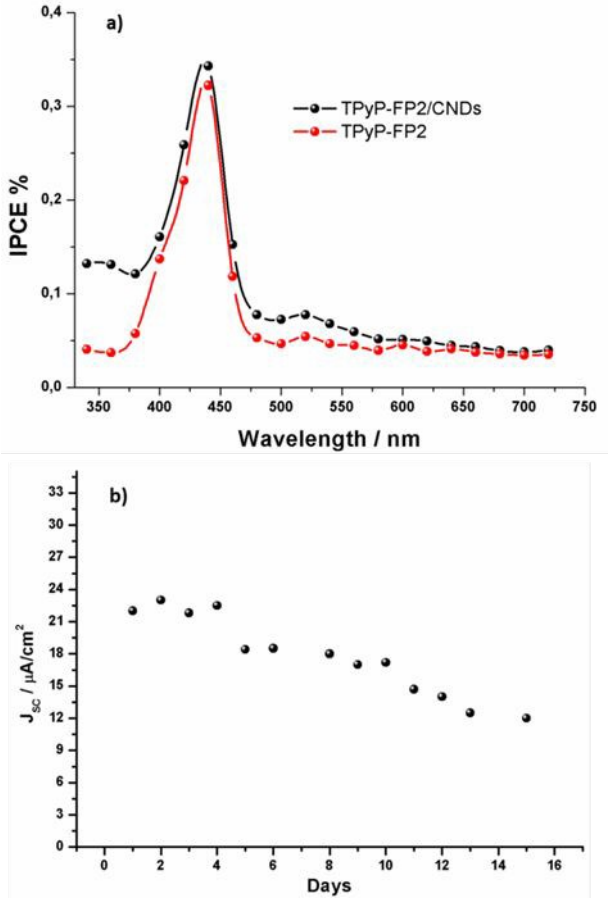


**Figure 10. a) Photoaction spectra of ITO/(TPyP-FP2)$_8$/I$^-$,I$_3^-$/Pt-ITO (red line) and ITO/(TPyP-FP2/CNDs)$_8$/I$^-$,I$_3^-$/Pt-ITO. The experiments were carried out at room temperature, a photoactive film surface area of 0.28 cm$^2$ was considered and the electrolyte composition was 0.5 M LiI, 0.01 M I$_2$ in acetonitrile. b) Stability of the photocurrent during 15 days when the device is dark stored at room temperature**

## Conclusions

Herein, negatively charged water soluble carbon dots were synthetized and used to promote a supramolecular adduct with doubly charged fulleropyrrolidine. Fluorescence quenching of CNDs, graphed according to the Stern-Volmer plot, in presence of FP2 follows a compressed-exponential growth, confirming the strong interaction between the two allotropic forms of carbon. FP2/CNDs adducts formed at the air/subphase interface were characterized by Brewster Angle Microscopy, Reflection Spectroscopy and by recording the surface pressure vs area per molecule Langmuir isotherms. The floating film was transferred onto ITO solid substrates by means of the Langmuir-Schaefer method.

Photoresponsivity of the FP2/CNDs dyad was evaluated assembling a thin film solar cell and a photoinduced charge separation demonstrated in the carbon dots/fullerene derivative composite film. The performances of LS TPyP-FP2 and TPyP-FP2/CNDs have been analyzed. An enhancement of about 160% of the short circuit current under illumination compared with FP2/CNDs and 290% when compared with TPyP-FP2 has been obtained opening interesting scenarios for improving the charge separation in light harvesting and solar energy conversion systems.

## Conflicts of interest

There are no conflicts to declare.

## Acknowledgements

This research was supported by “FutureInResearch” APQ Ricerca Regione Puglia and Programma Operativo Nazionale FSE-FESR Ricerca e Innovazione 2015-2020 – Asse prioritario I “Investimenti in Capitale Umano” - Azione I.1 – “Dottorati Innovativi con caratterizzazione industriale”, XXXII.

## References

1 M. Fathizadeh, W. L. Xu, F. Zhou, Y. Yoon and M. Yu, *Adv. Mater. Interfaces*, 2017, **4**, 1600918.
2 R. Imani, F. Mohabatpour and F. Mostafavi, *Carbon N. Y.*, 2018, **140**, 569–591.
3 D. Pech, M. Brunet, H. Durou, P. Huang, V. Mochalin, Y. Gogotsi, P.-L. Taberna and P. Simon, *Nat. Nanotechnol.*, 2010, **5**, 651–654.
4 O. Mykhailiv, H. Zubyk and M. E. Plonska-Brzezinska, *Inorganica Chim. Acta*, 2017, **468**, 49–66.
5 W. Zhai, N. Srikanth, L. B. Kong and K. Zhou, *Carbon N. Y.*, 2017, **119**, 150–171.
6 V. N. Mochalin, O. Shenderova, D. Ho and Y. Gogotsi, *Nat. Nanotechnol.*, 2012, **7**, 11–23.
7 S. Kumar, R. Rani, N. Dilbaghi, K. Tankeshwar and K.-H. Kim, *Chem. Soc. Rev.*, 2017, **46**, 158–196.
8 G. Giancane, S. Bettini and L. Valli, *Colloids Surfaces A Physicochem. Eng. Asp.*, 2010, **354**, 81–90.
9 S. Augustine, J. Singh, M. Srivastava, M. Sharma, A. Das and B. D. Malhotra, *Biomater. Sci.*, 2017, **5**, 901–952.
10 B. C. Thompson and J. M. J. Fréchet, *Angew. Chemie Int. Ed.*, 2008, **47**, 58–77.
11 C. Rizzo, F. Arcudi, L. Đorđević, N. T. Dintcheva, R. Noto, F. D’Anna and M. Prato, *ACS Nano*, 2018, **12**, 1296–1305.
12 R. Wang, K.-Q. Lu, Z.-R. Tang and Y.-J. Xu, *J. Mater. Chem. A*, 2017, **5**, 3717–3734.
13 F. Rigodanza, L. Đorđević, F. Arcudi and M. Prato, *Angew. Chemie Int. Ed.*, 2018, **57**, 5062–5067.
14 F. Arcudi, L. Đorđević and M. Prato, *Angew. Chemie Int. Ed.*, 2017, **56**, 4170–4173.
15 S. Y. Lim, W. Shen and Z. Gao, *Chem. Soc. Rev.*, 2015, **44**, 362–381.
16 Li Cao, Xin Wang, Mohammed J. Meziani, Fushen Lu, Haifang Wang, Pengju G. Luo, Yi Lin, Barbara A. Harruff, L. Monica Veca, Davoy Murray, A. Su-Yuan Xie and Y.-P. Sun*, *J. Am. Chem. Soc.*, 2007, **129**, 11318–11319.
17 R. Liu, D. Wu, S. Liu, K. Koynov, W. Knoll and Q. Li, *Angew. Chemie Int. Ed.*, 2009, **48**, 4598–4601.
18 D. Mo, L. Hu, G. Zeng, G. Chen, J. Wan, Z. Yu, Z. Huang, K. He, C. Zhang and M. Cheng, *Appl. Microbiol. Biotechnol.*, 2017, **101**, 2713–2733.
19 M. Albota, D. Beljonne, J. L. Brédas, J. E. Ehrlich, J. Y. Fu, A.

A. Heikal, S. E. Hess, T. Kogej, M. D. Levin, S. R. Marder, D. McCord-Maughon, J. W. Perry, H. Röckel, M. Rumi, G. Subramaniam, W. W. Webb, X. L. Wu and C. Xu, *Science (80-. ).*, 1998, **281**, 1653–1656.

20 S. Paulo, G. Stoica, W. Cambarau, E. Martinez-Ferrero and E. Palomares, *Synth. Met.*, 2016, **222**, 17–22.

21 H. Cao, S. Liu, W. Tu, J. Bao and Z. Dai, *Chem. Commun.*, 2014, **50**, 13315–13318.

22 X. Shen, B. Sun, D. Liu and S.-T. Lee, *J. Am. Chem. Soc.*, 2011, **133**, 19408–19415.

23 P. Mirtchev, E. J. Henderson, N. Soheilnia, C. M. Yip and G. A. Ozin, *J. Mater. Chem.*, 2012, **22**, 1265–1269.

24 Y.-Q. Zhang, D.-K. Ma, Y.-G. Zhang, W. Chen and S.-M. Huang, *Nano Energy*, 2013, **2**, 545–552.

25 R. Narayanan, M. Deepa and A. K. Srivastava, *J. Mater. Chem. A*, 2013, **1**, 3907.

26 S. Carrara, F. Arcudi, M. Prato and L. De Cola, *Angew. Chemie Int. Ed.*, 2017, **56**, 4757–4761.

27 L. Bao, Z.-L. Zhang, Z.-Q. Tian, L. Zhang, C. Liu, Y. Lin, B. Qi and D.-W. Pang, *Adv. Mater.*, 2011, **23**, 5801–5806.

28 F. Arcudi, V. Strauss, L. Đorđević, A. Cadranel, D. M. Guldi and M. Prato, *Angew. Chemie Int. Ed.*, 2017, **56**, 12097–12101.

29 A. Cadranel, V. Strauss, J. T. Margraf, K. A. Winterfeld, C. Vogl, L. Đorđević, F. Arcudi, H. Hoelzel, N. Jux, M. Prato and D. M. Guldi, *J. Am. Chem. Soc.*, 2018, **140**, 904–907.

30 M. C. Petty, *Langmuir-Blodgett films an introduction*, Cambridge University Press, Cambridge, 1996.

31 A. Mateo-Alonso, C. Sooambar and M. Prato, *Org. Biomol. Chem.*, 2006, **4**, 1629.

32 X. Dong, Y. Su, H. Geng, Z. Li, C. Yang, X. Li and Y. Zhang, *J. Mater. Chem. C*, 2014, **2**, 7477–7481.

33 R. Rella, A. Serra, P. Siciliano, A. Tepore, L. Valli and A. Zocco, *Supramol. Sci.*, 1997, **4**, 461–464.

34 G. Giancane, V. Borovkov, Y. Inoue, S. Conoci and L. Valli, *Soft Matter*, 2013, **9**, 2302.

35 H. Kuhn and D. Möbius, *Investigations of surfaces and interfaces*, Wiley-Interscience, New York, 1993.

36 S. Bettini, R. Pagano, L. Valli and G. Giancane, *J. Phys. Chem. C*, 2014, **118**, 12384–12390.

37 V. Sgobba, G. Giancane, S. Conoci, S. Casilli, G. Ricciardi, D. M. Guldi, M. Prato and L. Valli, *J. Am. Chem. Soc.*, 2007, **129**, 3148–3156.

38 V. Sgobba, G. Giancane, D. Cannoletta, A. Operamolla, O. Hassan Omar, G. M. Farinola, D. M. Guldi and L. Valli, *ACS Appl. Mater. Interfaces*, 2014, **6**, 153–158.

39 R. M. (Robert M. Silverstein, F. X. Webster, D. J. Kiemle and D. L. (David L. Bryce, *Spectrometric identification of organic compounds*, John Wiley & Sons, Ltd, 8th editio., 2014.

40 Y. Xu, M. Wu, Y. Liu, X.-Z. Feng, X.-B. Yin, X.-W. He and Y.-K. Zhang, *Chem. - A Eur. J.*, 2013, **19**, 2276–2283.

41 N. Arumugam and J. Kim, *Mater. Lett.*, 2018, **219**, 37–40.

42 S. Sahu, B. Behera, T. K. Maiti and S. Mohapatra, *Chem. Commun.*, 2012, **48**, 8835-8837.

43 M. Xue, Z. Zhan, M. Zou, L. Zhang and S. Zhao, *New J. Chem.*, 2016, **40**, 1698–1703.

44 H. Li, W. Kong, J. Liu, N. Liu, H. Huang, Y. Liu and Z. Kang, *Carbon N. Y.*, 2015, **91**, 66–75.

45 Z. Yang, M. Xu, Y. Liu, F. He, F. Gao, Y. Su, H. Wei and Y. Zhang, *Nanoscale*, 2014, **6**, 1890–1895.

46 K. K. Chan, S. H. K. Yap and K.-T. Yong, *Nano-Micro Lett.*, 2018, **10**, 72.

47 S. Zhu, Y. Song, X. Zhao, J. Shao, J. Zhang and B. Yang, *Nano Res.*, 2015, **8**, 355–381.

48 F. Arcudi, L. Đorđević and M. Prato, *Angew. Chemie Int. Ed.*, 2016, **55**, 2107–2112.

49 A. Sharma, T. Gadly, A. Gupta, A. Ballal, S. K. Ghosh and M. Kumbhakar, *J. Phys. Chem. Lett.*, 2016, **7**, 3695–3702.

50 Y. Su, M. Xie, X. Lu, H. Wei, H. Geng, Z. Yang and Y. Zhang, *RSC Adv.*, 2014, **4**, 4839-4842.

51 Y.-P. Sun, B. Zhou, Y. Lin, W. Wang, K. A. S. Fernando, P. Pathak, M. J. Meziani, B. A. Harruff, X. Wang, H. Wang, P. G. Luo, H. Yang, M. E. Kose, B. Chen, A. L. M. Veca and S.-Y. Xie, *J. Am. Chem. Soc.*, 2006, **128**, 7756–7757.

52 Y.-H. Chien, K. K. Chan, S. H. K. Yap and K.-T. Yong, *J. Chem. Technol. Biotechnol.*, 2018, **93**, 1519–1528.

53 X. Wen, P. Yu, Y.-R. Toh, X. Ma and J. Tang, *Chem. Commun.*, 2014, **50**, 4703–4706.

54 J. Joseph and A. A. Anappara, *J. Lumin.*, 2016, **178**, 128–133.

55 K. Linehan and H. Doyle, *RSC Adv.*, 2014, **4**, 12094–12097.

56 J. Gao, M. Zhu, H. Huang, Y. Liu and Z. Kang, *Inorg. Chem. Front.*, 2017, **4**, 1963–1986.

57 D. K. Singh, P. K. Iyer and P. K. Giri, *Carbon N. Y.*, 2012, **50**, 4495–4505.

58 R. Das, G. Rajender and P. K. Giri, *Phys. Chem. Chem. Phys.*, 2018, **20**, 4527–4537.

59 K. Dimos, F. Arcudi, A. Kouloumpis, I. B. Koutselas, P. Rudolf, D. Gournis and M. Prato, *Nanoscale*, 2017, **9**, 10256–10262.

60 S. Bettini, R. Pagano, V. Bonfrate, E. Maglie, D. Manno, A. Serra, L. Valli and G. Giancane, *J. Phys. Chem. C*, 2015, **119**, 20143–20149.

61 K. Ariga, H. Ito, J. P. Hill and H. Tsukube, *Chem. Soc. Rev.*, 2012, **41**, 5800-5835.

62 G. Giancane, V. Borovkov, Y. Inoue, S. Conoci and L. Valli, *Soft Matter*, 2013, **9**, 2302-2307.

63 G. Giancane, L. Valli and S. Sortino, *ChemPhysChem*, 2009, **10**, 3077–3082.

64 S. Bettini, L. Valli, A. Santino, C. Martinelli, G. M. Farinola, A. Cardone, V. Sgobba and G. Giancane, *Dye. Pigment.*, 2012, **94**, 156–162.

65 K. Ariga, T. Mori, W. Nakanishi and J. P. Hill, *Phys. Chem. Chem. Phys.*, 2017, **19**, 23658–23676.

66 G. Yu, K. Jie and F. Huang, *Chem. Rev.*, 2015, **115**, 7240–7303.

67 S. Bettini, R. Pagano, V. Borovkov, G. Giancane and L. Valli, *J. Colloid Interface Sci.*, 2019, **533**, 762–770.

68 A. Buccolieri, S. Bettini, L. Salvatore, F. Baldassarre, G. Ciccarella and G. Giancane, *Sensors Actuators B Chem.*, 2018, **267**, 265–271.

69 K. L. Chen and M. Elimelech, *Langmuir*, 2006, **22**, 10994–11001.

70 L. Pospíšil, M. Gál, M. Hromadová, J. Bulíčková, V. Kolivoška, J. Cvačka, K. Nováková, L. Kavan, M. Zukalová and L. Dunsch, *Phys. Chem. Chem. Phys.*, 2010, **12**, 14095.

71 M. Maggini, L. Pasimeni, M. Prato, G. Scorrano and L. Valli, *Langmuir*, 1994, **10**, 4164–4166.

72 A. Privitera, M. Righetto, D. Mosconi, F. Lorandi, A. A. Isse, A. Moretto, R. Bozio, C. Ferrante and L. Franco, *Phys. Chem. Chem. Phys.*, 2016, **18**, 31286–31295.

73 X. Sun, L. Y. Ji, W. W. Chen, X. Guo, H. H. Wang, M. Lei, Q. Wang and Y. F. Li, *J. Mater. Chem. A*, 2017, **5**, 20720–20728.

View Article Online
DOI: 10.1039/C9NR00951E

74 W. Andreoni, in *Physics and Chemistry of the Fullerenes*, ed. K. Prassides, Springer Netherlands, Dordrecht, 1994, pp. 169–182.
75 S. Paulo, G. Stoica, W. Cambarau, E. Martinez-Ferrero and E. Palomares, *Synth. Met.*, 2016, **222**, 17–22.
76 H. Imahori, *Bull. Chem. Soc. Jpn.*, 2007, **80**, 621–636.
77 D. M. Guldi, *J. Phys. Chem. B*, 2005, **109**, 11432–11441.
78 T. Hasobe, P. V. Kamat, M. A. Absalom, Y. Kashiwagi, J. Sly, M. J. Crossley, K. Hosomizu, H. Imahori and S. Fukuzumi, *J. Phys. Chem. B*, 2004, **108**, 12865–12872.
79 S. Bettini, R. Pagano, L. Valli and G. Giancane, *J. Phys. Chem. C*, , DOI:10.1021/jp503292r.
80 L. A. Valkova, L. Valli, S. Casilli, G. Giancane, N. Y. Borovkov, G. V. Sibrina, A. S. Glibin, O. I. Koifman, M. Pisani and F. Rustichelli, *Langmuir*, 2008, **24**, 4857–4864.